Metacognitive ability predicts hippocampal and prefrontal microstructure

Micah Allen[1,2], James C. Glen[1], Daniel Müllensiefen[3], Dietrich Samuel Schwarzkopf[1,4], Martina F. Callaghan[2], Geraint Rees[1,2]

[1]Institute of Cognitive Neuroscience, UCL
[2]Wellcome Trust Center for Neuroimaging at UCL
[3]Department of Psychology, Goldsmiths, University of London
[4]Experimental Psychology, 26 Bedford Way, WC1H 0AP

Abstract:

The ability to introspectively evaluate our experiences to form accurate metacognitive beliefs, or insight, is an essential component of decision-making. Previous research suggests individuals vary substantially in their level of insight, and that this variation predicts brain volume and function, particularly in the anterior prefrontal cortex (aPFC). However, the neurobiological mechanisms underlying these effects are unclear, as qualitative, macroscopic measures such as brain volume can be related to a variety of microstructural features. Here we used a newly developed, high-resolution (800μm isotropic) multi-parameter mapping technique in 48 healthy individuals to delineate quantitative markers of *in vivo* histological features underlying metacognitive ability. Specifically, we examined how neuroimaging markers of local grey matter myelination, macromolecular and iron content relate to insight. Extending previous volumetric findings, we found that metacognitive ability, as determined by a signal-detection theoretic model, was positively related to the myelo-architectural integrity of aPFC grey matter. Interestingly, perceptual metacognition predicted decreased macromolecule content coupled with increased iron in the hippocampus and precuneus, areas previously implicated in meta-memory rather than meta-perception. Further, the relationship of hippocampal-precuneus and prefrontal microstructure to an auditory memory measure was respectively mediated or suppressed by metacognitive ability, suggesting a dynamic trade-off between participant's memory and metacognition. These results point towards a novel understanding of the relationship between memory, brain microstructure, and metacognition.

Significance Statement:

By combining a signal-theoretic model of individual metacognitive ability with state of the art quantitative neuroimaging, our results shed new light on the neurobiological mechanisms underlying introspective insight. Myelination and iron are core determinants of both healthy brain maturation and neurodegeneration; particularly in the hippocampus where iron accumulation is linked to oxidative stress and inflammation. Our results may thus indicate that metacognition depends upon the development and integrity of a memory-related brain network, potentially revealing novel biomarkers of neurodegeneration. These results highlight the power of quantitative mapping to reveal neurobiological correlates of behaviour.

SUBMITTED TO JOURNAL OF NEUROSCIENCE

Introduction

The metacognitive capacity for self-monitoring is at the core of learning and decision-making (Flavell, 1979). As a general capacity, metacognition is thought to enable the flexible monitoring and control of memory, perception and action (Fernandez-Duque et al., 2000). An efficient approach to quantifying this ability lies in the application of signal-detection theory to estimate the sensitivity of self-reported confidence to objective discrimination performance (Fleming and Lau, 2014). Individual differences in metacognitive sensitivity thus quantified are related to the morphological structure, function, and connectivity of the brain (for review, see Fleming and Dolan, 2012). Here we expand on these findings using a newly developed multi-parameter mapping (MPM) and voxel-based quantification (VBQ) technique to better elucidate the neurobiological mechanisms underpinning these effects.

The anterior prefrontal cortex (aPFC) (Fleming et al., 2010, 2012, 2014; Sinanaj et al., 2015) and precuneus (Baird et al., 2013; McCurdy et al., 2013) have been repeatedly related to metacognitive ability. Notably, several studies found a positive relationship between right APFC volume and metacognition (Fleming et al., 2010; McCurdy et al., 2013; Sinanaj et al., 2015). While convergent evidence from anatomical, lesion-based, and functional connectivity studies suggest that the right aPFC is specific to perceptual metacognition, metacognition for memory has instead been related to midline cortical (e.g., mPFC and PCC/precuneus) and hippocampal structures. (Fleming et al., 2012, 2014; Baird et al., 2013; McCurdy et al., 2013). Although these studies suggest that the ability to introspect on perception and memory depends on the development of a neural mechanism involving both domain-specific and general aspects, the underlying neurobiology driving the relationship between neuroanatomy and metacognition remains unclear.

This uncertainty lies partly in the inherent lack of specificity offered by volumetric measures of brain structure, which are fundamentally qualitative in nature. Indeed, voxel-based

morphometry (VBM) yields measures in arbitrary units which can be driven by a variety of macroscopic factors such as cortical thickness and variability in cortical folding, owing to a non-specific variety of microstructural features (Ashburner, 2009). It has recently been shown that microstructural properties of brain tissue, such as myelination levels and iron content can lead to the detection of spurious morphological changes (Lorio et al., 2014, 2016). The emerging field of *in vivo* histology aims to combine maps of specific MRI parameters measured via quantitative imaging (qMRI) with biophysical models to provide direct indicators of the microstructural mechanisms driving morphological findings, and ultimately to quantify biologically relevant metrics such as myelination and iron concentrations, oligodendrocyte distributions, and the g-ratio of fibre pathways (Mohammadi et al., 2015; Weiskopf et al., 2015).

In the present study we used qMRI to map a number of key contrast parameters with differential sensitivity to underlying biological metrics, in order to better understand the microstructural correlates of metacognitive ability. To do so, we acquired high-resolution (800µm isotropic) data using the Multi-Parametric Mapping (MPM) qMRI protocol (Weiskopf et al., 2013). Respecting the quantitative nature of these data, we conducted voxel-based quantification (VBQ) analysis (Draganski et al., 2011) in 48 healthy participants to relate these microstructural markers to individual differences in metacognitive sensitivity during an adaptive visual motion discrimination task. Our results confirmed that right aPFC markers of myelo-architecture positively predict metacognitive ability, whereas left hippocampus and precuneus showed effects consistent with both decreased macromolecule and increased iron content. Further clarifying the domain-general role of memory in metacognition, the relationship of hippocampus and precuneus microstructure with auditory memory was mediated by metacognitive ability. These results extend our understanding of the

92 computational neuroanatomy of metacognition and provide novel targets for future clinical
93 research.
94
95 **Methods**
96 *Participants*
97 48 healthy participants (29 female) were recruited from University College London and the
98 surrounding community. As age is a strong determinant of micro-architecture and grey matter
99 volume (Callaghan et al., 2014), we restricted our inclusion criteria to 20-40 years, resulting in
100 a mean age of 24 (SD = 5). All participants were right handed, and were mentally and
101 physically healthy with no history of neurological disorders and with normal (or corrected-to
102 normal) vision and hearing. Participants were recruited from a local participant database using
103 broadcast emails. All participants gave informed written consent to all procedures. In
104 accordance with the Declaration of Helsinki, the University College London Research Ethics
105 Committee approved all procedures.
106
107 *Study Design*
108 Participants completed the experiment in two sessions, consisting of a 2-hour appointment at
109 the Wellcome Trust Center for Neuroimaging to acquire all imaging data, and a separate 1-
110 hour appointment to complete the metacognition task, a brief non-verbal auditory memory
111 measure (Müllensiefen et al., 2014), and other behavioural measures (data not reported here).
112 The neuroimaging session involved 30 minutes of multi-parameter mapping (MPM) while
113 subjects silently viewed a muted nature documentary (to promote stillness). During the
114 behavioural session, participants completed an adaptive psychophysical visual metacognition
115 task (see *Behaviour*, below) lasting 30 minutes.
116

Behaviour – Metacognition Global Motion Task

To measure participants' metacognitive ability, we employed a global dot motion discrimination task comprising a forced-choice motion judgement with retrospective confidence ratings on every trial. As part of another investigation, in which we were investigating noise-induced confidence bias (Spence et al., 2015), we used a dual-staircase approach with two conditions in which either mean direction or standard deviation across dot directions was continuously adapted to stabilize discrimination performance. Thus, to control sensory noise independently of task difficulty, in two randomly interleaved conditions we presented either a stimulus with a fixed 15-degree mean angle of motion from vertical and a variable (adaptive) standard deviation (SD), or a variable (adaptive) mean angle from vertical at a fixed 30 degree SD. In either case, the mean (μ-staircase condition, μ*S*) or standard deviation (σ-staircase condition, σ*S*) of motion was continuously adjusted according to a 2-up-1 down staircase, which converges on 71% performance. On each trial the motion signal was thus constructed using the formula:

DotDirections = Direction (Left vs Right) * MeanOrientation + GaussianNoise*SD

In which the condition-specific staircase determined either mean orientation or SD. Each trial consisted of a 500ms fixation, followed by a 250ms central presentation of the motion stimulus, which was then replaced by a central letter display "L R". Participants then had 800ms to make their response to indicate whether the mean motion direction was to the left or right of vertical. After this, a confidence rating scale marked by 4 equal vertical lines appeared. Each line was labelled, from left to right "no confidence, low, moderate, high confidence. Participants' heads were fixed with a chin and forehead rest 72 cm from the screen. Motion stimuli consisted of a central array of 1,100 dots presented over a central fixation dot, within a circular aperture of

radius 9.5 degrees visual angle (DVA), with dots advancing 0.02 DVA per frame. To ensure participants attended the global rather than the local motion direction, dot lifetimes were randomized and limited to a maximum of 93% stimulus duration.

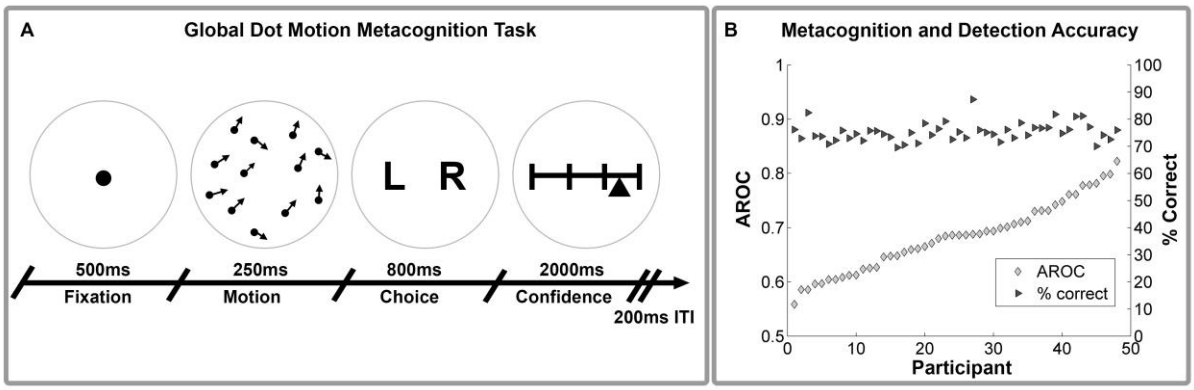

Figure 1, **Behavioral Paradigm and Metacognitive Accuracy.** Schematic of global dot-motion metacognition task (A) and plot of metacognitive vs motion detection accuracy (B). Participants were required to judge the global or average motion of a brief dot display, and then rate their confidence in this judgement from 0 (guessing) to 100 (certain). Performance was held constant using an adaptive threshold adjusting either signal mean or variance on each trial (see *Methods* for more details). Right hand plot demonstrates substantial individual differences in metacognitive accuracy, estimated as the type-II area under the curve (AROC), independently of motion discrimination performance. Inter-individual differences in AROC were then used in a multiple regression analysis to explain variation in microstructural brain features (see *VBQ Analysis*).

Participants were instructed that the goal of the task was to measure their perceptual and metacognitive ability. Metacognitive ability was defined as a participant's insight into the correctness of their motion judgements, i.e. how well their confidence reports reflected their discrimination accuracy. Participants completed a short practice block of 56 trials, in which they performed the motion discrimination without confidence ratings, with choice accuracy feedback provided by changing the colour of the fixation to green or red. All participants achieved better than 70% accuracy and indicated full understanding of the task before continuing. Participants completed 320 trials divided evenly between the two staircase

conditions. Trials were divided into 10 blocks each with 40 trials, randomly interleaved across conditions within each block. 14 participants did not complete the last two blocks of the task due to a technical error, however all participants had at least 100 trials per condition (Fleming and Lau, 2014).

Non-Verbal Auditory Measure

As previous studies have found both commonalities and differences between metacognition for perception and memory (Baird et al., 2013; McCurdy et al., 2013), we collected a brief measure of participant's non-verbal auditory memory using a common same-different comparison paradigm (Müllensiefen et al., 2014). This involved a short AB task in which participants listened to a sequence of 10-17 notes, and then decided if a subsequent sequence at a different absolute pitch level had the same or a different structure. The second note sequence was always transposed either by a fifth or by a semitone. Participants were required to indicate whether the two note sequences had an identical pitch interval structure or not. The test score was then calculated as the accuracy of the same-different judgement for each participant across all 13 trials.

Quantitative Multi-Parameter Mapping (MPM)

Recent technical developments have enabled *in vivo* mapping of neuroimaging markers of biologically relevant quantities to be performed with high resolution and whole brain coverage (Deoni et al., 2005; Helms et al., 2008a, 2008b, 2009). We used the Multi-Parameter Mapping (MPM) protocol (Weiskopf et al., 2013) to obtain maps of the percent saturation due to magnetization transfer (MT), longitudinal relaxation rate (R_1), and effective transverse relaxation rate (R_2*).

Data Acquisition

All imaging data were collected on a 3T whole body MR system (Magnetom TIM Trio, Siemens Healthcare, Erlangen, Germany) using the body coil for radio-frequency (RF) transmission and a standard 32-channel RF head coil for reception. A whole-brain quantitative MPM protocol consisting of 3 spoiled multi-echo 3D fast low angle shot (FLASH) acquisitions with 800 µm isotropic resolution and 2 additional calibration sequences to correct for inhomogeneities in the RF transmit field (Lutti et al., 2010, 2012; Callaghan et al., 2015b).

The FLASH acquisitions had predominantly proton density (PD), T1 or MT weighting. The flip angle was 6^0 for the PD- and MT-weighted volumes and 21^0 for the T1 weighted acquisition. MT-weighting was achieved through the application of a Gaussian RF pulse 2 kHz off resonance with 4ms duration and a nominal flip angle of 220^0. The field of view was 256mm head-foot, 224mm anterior-posterior (AP), and 179mm right-left (RL). Gradient echoes were acquired with alternating readout gradient polarity at eight equidistant echo times ranging from 2.34 to 18.44ms in steps of 2.30ms using a readout bandwidth of 488Hz/pixel. Only six echoes were acquired for the MT-weighted acquisition in order to maintain a repetition time (TR) of 25ms for all FLASH volumes. To accelerate the data acquisition, partially parallel imaging using the GRAPPA algorithm was employed with a speed-up factor of 2 in each phase-encoded direction (AP and RL) with forty integrated reference lines.

To maximise the accuracy of the measurements, inhomogeneity in the transmit field was mapped using the 2D STEAM approach described in Lutti *et al.* 2010, including correcting for geometric distortions of the EPI data due to B0 field inhomogeneity. Total acquisition time for all MRI scans was less than 30 mins.

Parameter Map Estimation and Voxel-Based Quantification (VBQ)

All images were processed using SPM12 (version 12.2, Wellcome Trust Centre for Neuroimaging, http://www.fil.ion.ucl.ac.uk/spm/) and bespoke tools implemented in the voxel-based quantification (VBQ) toolbox version 2e (Draganski et al., 2011; Weiskopf et al., 2015), implemented in MATLAB (Mathworks Inc, version R2014a).

To create the quantitative maps, all weighted volumes were co-registered to address inter-scan motion. Maps of R_2* were estimated from the gradient echoes of all contrasts using the ordinary least squares ESTATICS approach (Weiskopf et al., 2014). The image data for each acquired weighting (PDw, T1w, MTw) were then averaged over the first six echoes to increase the signal-to-noise ratio (SNR) (Helms et al., 2009). The three resulting volumes were used to calculate MT and R_1 as described in (Helms et al., 2008a, 2008b) including corrections for transmit field inhomogeneity and imperfect spoiling (Preibisch and Deichmann, 2009a, 2009b; Callaghan et al., 2015c). The MT map depicts the percentage loss of signal (MT saturation) that results from the application of the off-resonance MT pre-pulse and the dynamics of the magnetization transfer (Helms et al., 2008b).

A Gaussian mixture model implemented within the unified segmentation approach was used to classify MT maps into grey matter (GM), white matter (WM) and cerebrospinal fluid (CSF) (Ashburner and Friston, 2005). Diffeomorphic image registration (DARTEL) was used to spatially normalise individual grey and white matter tissue classes generated from the structural MT maps to a group mean template image (Ashburner, 2007). The resulting DARTEL template and participant-specific deformation fields were used to normalise the MT, R_1 and R_2* maps of each participant to standard MNI space. We based our normalization of the quantitative map on the MT maps because of their greatly improved contrast in subcortical structures, e.g. basal ganglia, and similar WM/GM contrast in the cortex to T1-weighted images (Helms et al., 2008a). A 4 mm full-width at half-maximum (FWHM) Gaussian smoothing kernel was applied to the R_1, MT, and R_2* during normalisation using the VBQ approach,

which aims to minimise partial volume effects and optimally preserve the quantitative values (Draganski et al., 2011). This tissue-specific approach to smoothing generates grey and white matter segments for each map. The grey matter segments were used in all subsequent analyses. For results visualization, an average MT map in standard MNI space was created from all participants.

Analysis

Behavioural Analysis – Detection Performance and Metacognitive Ability

All behavioural data were pre-processed using MATLAB (The Mathworks Inc, Natick, MA, USA). Following previous investigations, we discarded the first block of trials to allow for staircase stabilization. Any trial with reaction times (RT) below 100ms or more extreme than 3 SD of mean RT was rejected from analysis. To quantify metacognitive ability, we estimated the type-II area under the receiver-operating curve (AROC) (Fleming et al., 2010, 2012; Fleming and Lau, 2014) separately for each staircase condition. This method has been described extensively elsewhere (Fleming et al., 2010; Fleming and Lau, 2014), but briefly it involves constructing a receiver-operating curve describing the p(high confidence | correct response) vs the p(low confidence | incorrect response). Under equal performance the AROC thus describes the sensitivity of a participant's confidence ratings relative to their actual performance. For AROC estimation, confidence ratings were binned into 4 equally sized quartiles (a necessary step for fitting the signal-theoretic model) using bespoke MATLAB code. As a general index of metacognitive ability, we then calculated average AROC, as well as average confidence, mean accuracy (% correct responses), detection sensitivity (*d'*), choice bias (*c*), and reaction time (*RT*). We also calculated median signal mean, median signal variance, and accuracy within each condition to characterize our thresholding procedure.

VBQ Analysis – Metacognitive Ability

We initially focused on replicating and extending previous volumetric findings relating metacognitive ability to neuroanatomy (Fleming et al., 2010, 2014; McCurdy et al., 2013, 2013; Sinanaj et al., 2015). To do so we conducted volume of interest (VOI) multiple regression analyses using 5mm-radius spherical VOIs centred on the peak coordinates reported by Fleming (2010) and McCurdy (2013). This involved the creation of VOIs in the left (-20, 53, 12), (-12, 54, 16) and right (24, 65, 18), (33, 50, 9), (32, 50, 7) APFC, right dorsolateral PFC (36, 39, 21), and precuneus (6, -57, 18), (8, -64, 24). All VOIs were generated using the WFU Pickatlas Version 3.0.5 (Maldjian et al., 2003), and combined into a single mask. The resulting mask is available for download at Neurovault.org (http://neurovault.org/collections/1260/). We then modelled inter-subject variation in the MT, R_2*, and R1 grey matter maps in separate random-effects multiple regression analyses, modelling average AROC as our key dependent variable. Importantly, we followed previous investigations and controlled all analyses for average discrimination sensitivity (d-prime), confidence, response bias, the variance-induced confidence bias, and the difference in mean signal between the two staircases. To estimate variance-induced confidence bias, we fit multiple regression models within each subject, modelling trial-wise mean, variance, accuracy, and RT as predictors of confidence. This provided beta-weights for each participant indicating the degree to which their confidence report reflected variance-specific bias independently of the other modelled factors, which were then included in our VBQ multiple regression.

Following standard VBM procedure, we also included age, gender, and total intracranial volume as nuisance covariates. We then conducted small-volume corrected analyses of the positive and negative main effect of metacognitive ability (AROC) within our *a priori* mask, correcting for multiple comparisons using Gaussian Random Field Theory, FWE-peak

corrected alpha = 0.05. Further, we analysed the whole-brain maps of the same contrasts, using a non-stationarity corrected FWE-cluster p-value with a $p < 0.001$ inclusion threshold (Ridgway et al., 2008; Hupé, 2015). All anatomical labels and % activations were determined using the SPM Anatomy Toolbox (Eickhoff et al., 2005).

Mediation Analysis of Auditory Memory and Metacognition

To explore the relationship of metacognition, memory, and brain microstructure we conducted a single-level mediation analysis with the auditory memory score (*X*) predicting brain microstructure (*Y*), mediated by metacognitive ability (*M*) (Wager et al., 2009; Woo et al., 2015). This enabled us to infer whether the relationship of, e.g., hippocampal microstructure and memory depended upon metacognition. For this analysis, R_2* and MT values were extracted from each subject within the peak coordinate identified by our multiple-regression analysis, for the APFC (MT only), precuneus, and left hippocampus (see *VBQ Results*, below). As we observed a similar pattern of correlation for AROC in both hippocampus and precuneus, we first assessed the degree of correlation between each region for R_2* and MT, respectively. Indeed, R_2* and MT were significantly correlated between both regions (R_2* between region $R = 0.37$, $p = 0.009$; MT between region $R = 0.46$, $p = 0.002$). We thus averaged the values of each parameter across regions to create a general hippocampal-precuneus (HP) index for both measures. We then fit single-level mediation analyses using the Multilevel Mediation and Moderation Toolbox for MATLAB (https://github.com/canlab/MediationToolbox) to HP R_2*, HP MT, and APFC MT while controlling for the same covariates as in our VBQ analysis. Group-level significance for all direct (*a,b,c,c'*) and mediation parameters (*ab*) was assessed using a bootstrapping procedure with 10,000 bootstrap samples, alpha = 0.05.

Results

316

317 ***Behavioural Results***

318 To check staircase stability, we first performed two-way repeated measures ANOVA (factor
319 A: block, levels 1-7; Factor B: staircase condition, μ*S* *vs* σ*S*) on accuracy scores after removing
320 the first block. As several subjects did not complete the last two blocks, we first re-binned trials
321 into 8 equal size bins of 20% total trial length, before analysing block stability. This analysis
322 revealed a significant main effect of variance on accuracy ($F(1, 47) = 15.15$, $p < 0.001$), but no
323 main effect of block (*ps* > *.33*) or block by condition interaction ($p > 0.11$), indicating that
324 although average performance was slightly higher in the σ*S* condition (Mean Accuracy μ*S* =
325 73.4%, Mean Accuracy σ*S* = 76.6%), this difference did not change over time, indicating stable
326 performance within each staircase. As a further check we repeated this analysis separately
327 within each condition; in both cases the block main effect was not significant (all *ps* > 0.13).
328 All participants thus achieved stable performance, with an average accuracy of 75.3% (SD =
329 3%) across two conditions. Metacognitive ability was comparable to previous studies using the
330 AROC (mean AROC = 0.68, SD = 0.06) and did not differ between conditions, $t(47) = -0.67$,
331 p = 0.51. Table 1 presents descriptive statistics for discrimination and metacognition
332 performance.

333

334 ***Neuroimaging Results***

335

336 *VOI analysis – extension of previous APFC and precuneus Findings*

337 Our VOI analysis revealed significant correlations within the right precuneus and aPFC. aPFC
338 showed overlapping, significant positive correlations of AROC with both R_1 (peak voxel
339 MNI_{xyz} = [37 41 22]) and MT (peak voxel MNI_{xyz} = [37 42 22]) maps. As both maps are
340 sensitive to myelination to a varying degree, this suggests previous volumetric findings in the

aPFC are related to the myelo-architecture of the cortical grey matter. In contrast, in the precuneus we found that AROC was negatively related to MT (peak voxel MNI_{xyz} = [10 -58 8]) and positively related to R_2* (peak voxel MNI_{xyz} = [9 -64 24]). This result likely indicates a complex interaction between iron-regulating macromolecules such as ferritin, microglia, or amybetaloids and local iron concentration (Galazka-Friedman et al., 2009). Interestingly, it may explain why some previous studies failed to find correlates of perceptual metacognition in the precuneus (Fleming et al., 2010; Sinanaj et al., 2015), as this pattern of microstructural changes may counteract resulting in minimal contrast on T1-weighted images (Callaghan et al., 2015a) and therefore no net difference in a VBM analysis using such images. See table 2 and Figure 3 for summary of these results.

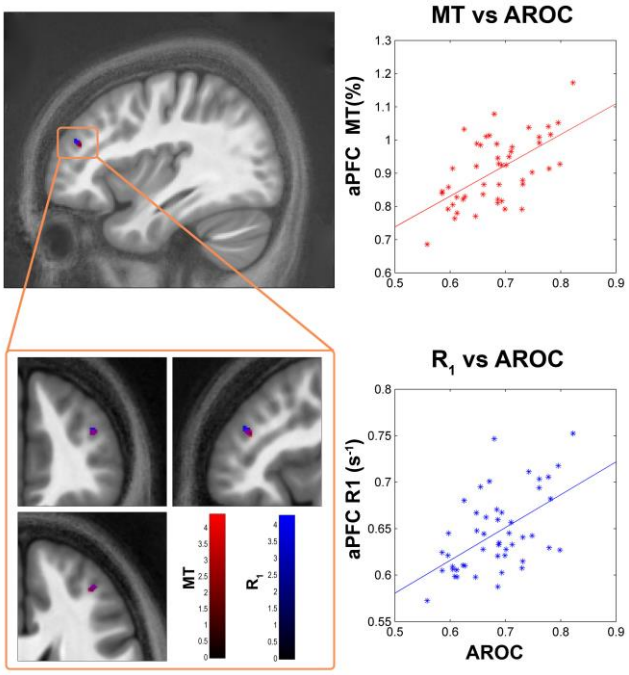

Figure 2 aPFC VBQ findings. Figure shows correlation of metacognitive ability (AROC) and anterior prefrontal (aPFC) microstructural measures of white-matter concentration (R_1 and MT) across 48 participants. Right side, scatter plots showing peak voxel vs AROC, with least-squares line for illustration purposes. Bottom left, zoomed in view shows overlap of AROC correlation in both MT and R_1 maps. Colour bars indicate t-values, blobs displayed on average MT map from our 48 participants. Volume of interest analysis, FWE-peak corrected $p < 0.05$ within mask generated from previously reported coordinates (Fleming et al., 2010; McCurdy et al., 2013). See *VBQ Analysis* for more details.

Whole-brain AROC Analysis

Our whole brain analysis revealed a striking relationship between AROC and left hippocampal MT. Here, higher AROC related to reduced MT in the left posterior-hippocampus (peak voxel MNI_{xyz} = [-31 -25 -14]). Inspection of this result in the SPM anatomy toolbox revealed that the majority (51.6%) was in the dentate gyrus (33.4% 'activated'), with another 29.3% in CA1 (14.2% activated), and to a lesser extent in the subiculum (6.6%, 1.8% activated) and CA3 (5.6%, 14.9% activated). Additionally, we found that iron levels as indexed by R_2* negatively predicted AROC in the visual cortex, primarily in V1 (peak voxel MNI_{xyz} = [1 -69 11]), and positively predicted AROC in the left middle-temporal gyrus (peak voxel MNI_{xyz} = [-51 -48 2]). A positive iron effect which was just above our cluster-level threshold (pFWE cluster = 0.052), but which was FWE-peak significant (pFWE peak = 0.044) was also found in the right subiculum (peak voxel MNI_{xyz} = [14 -38 -5]). Finally, as our VOI analysis indicated an inverse relationship between precuneus MT and R_2*, we were interested to see if a similar pattern could be found in the left hippocampus at a reduced (i.e., more exploratory) threshold. We thus lowered our uncorrected inclusion threshold to $p < 0.01$, FWE-cluster corrected to $p < 0.05$, and found that left hippocampal R_2* also positively predicted AROC (peak voxel MNI_{xyz} = [-26 -36 -13], pFWE < 0.001). These results are particularly interesting in light of the fact that they have not been previously reported in the context of perceptual metacognition, which may be due to the fact that decreased macromolecular content coupled with increased iron content may result in no net volume change being identified, highlighting the increased sensitivity and specificity of our method. All raw t-maps and FWE-thresholded maps have been made available to view and freely downloaded at Neurovault (http://neurovault.org/collections/1260/).

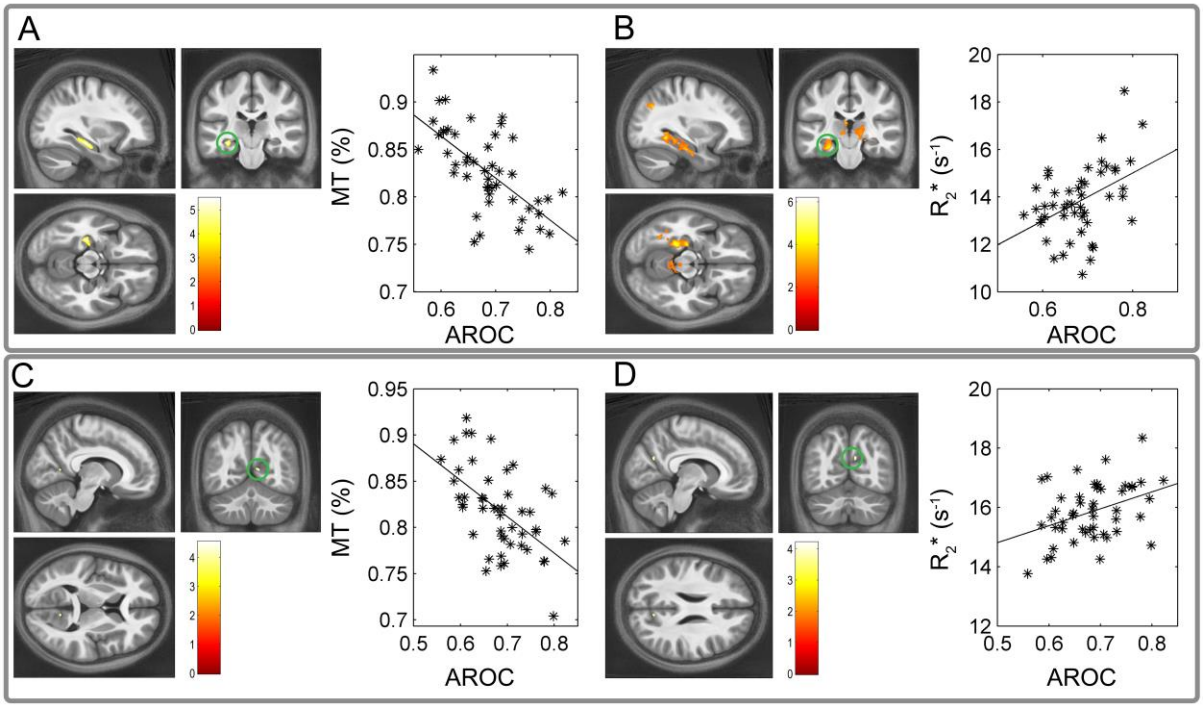

Figure 3, Hippocampus and Precuneus VBQ findings.

Voxel-based quantification results in the left hippocampus and right precuneus. Hippocampus MT negatively relates to metacognitive ability (AROC) (top left, A), whereas iron levels in the same region positively predict metacognition (top right, B). Interestingly, the same pattern is seen for right hippocampus. Blobs depict results of multiple regression analyses vs each map type, while controlling for age, gender, ICV, and a variety of performance-related variables (see *Methods* for more information). Results shown on average MT map in MNI space. Scatterplots are for illustration purposes only and depict the peak voxel from each SPM versus raw AROC. Top panel results are from FWE-cluster corrected whole brain analysis, pFWE < 0.05; bottom panel results are from VOI analysis across multiple regions drawn from previous volumetric metacognition studies.

Mediation Results - Auditory Memory and Metacognition

This analysis revealed a significant relationship between memory scores and AROC (mean path = 0.39, SD = 0.17, $p < 0.05$). Across all three brain measures, AROC significantly mediated the relationship of brain microstructure and memory ability – interestingly for MT this relationship was positive for the aPFC, with higher metacognition mediating the relationship of memory and aPFC (mean path = 0.24, SD = 0.15, $p < 0.05$); instead suppression (negative mediation) was observed for hippocampal-precuneus (mean path = -0.34, SD = 0.16, $p < 0.05$). Finally, for HP R_2* AROC also showed a positive mediation effect (mean path =

405 0.27, SD = 0.16, $p < 0.05$). These results suggest that metacognition differentially changes the
406 interrelation of prefrontal and hippocampal microstructure to memory ability, perhaps
407 indicating that individuals who are better at metacognition have a more 'metacognitive'
408 memory network and conversely, a more memory-related metacognition system. See figure 4
409 for an overview of these results.
410

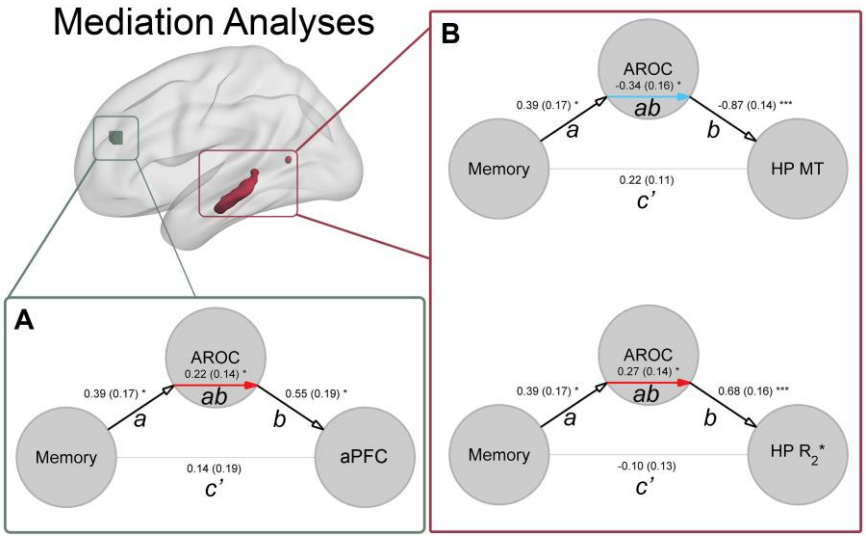

411

412 **Figure 4, Memory and Metacognition Mediation Analysis Results. A)** Metacognitive
413 ability (AROC) significantly mediates (red arrow) the relationship of non-verbal auditory
414 memory and APFC myelo-architecture (as measured by Magnetization Transfer Ratio, MT).
415 In contrast, **B)** the relationship of memory and hippocampal-precuneus (HP) myelo-
416 architecture is supressed by metacognitive ability (blue arrow), but enhanced for HP iron (as
417 measured by R_2*). These results suggest individual differences in memory and metacognition
418 are related by a dynamic interaction between the two networks, with the memory-related
419 network increasingly related to metacognitive circuits and vice versa for the prefrontal cortex.
420 Statistical significance for each parameter of the path model (*a*, *b*, *ab*, and *c';* * < 0.05, *** <
421 0.001) determined via bootstrapping procedure, see *Methods* for more details.
422

423 **Discussion**

424 Our findings demonstrate that individual differences in metacognitive ability are related to
425 underlying microstructural features of prefrontal and hippocampal neuroanatomy. Previous
426 studies investigating individual metacognitive ability indicated that the function, connectivity,
427 and volume of anterior prefrontal cortex (aPFC) underlie introspective insight. Here we build

on these findings using a novel quantitative magnetic resonance technique to show that prefrontal correlates of metacognition are related to markers of grey-matter myelo-architecture, as indexed by the overlapping effect in both MT and R_1 maps. In contrast, we found that differences consistent with decreased hippocampus and precuneus macromolecular content, coupled with increased iron content predicted metacognitive ability. Interestingly, we also found that metacognition mediated the relationship of memory ability and microstructure in the hippocampus and prefrontal cortex, suggesting a domain-general mechanism linking memory and metacognition. These results suggest that unique neurobiological mechanisms underlie the development and aetiology of metacognition for memory (i.e., meta-memory) and perception (meta-perception).

Previous investigations of metacognitive ability and individual differences in brain anatomy suggest that introspection for memory and perception depend upon both common and unique neural substrates. As strong evidence for their dissociation, Fleming et al (2014) recently demonstrated that medial-prefrontal (MPFC) or aPFC lesions selectively disrupt meta-memory or perception, respectively. In another study by McCurdy et al (2013), although metacognition for perception and memory were found to correlate, the two processes independently related to the volume of aPFC and precuneus. Interestingly, in an interaction analysis these authors found that while precuneus volume also predicted meta-perceptual ability, aPFC did not predict meta-memory. In contrast, Baird and colleagues (2013) found no behavioural correlation of meta-memory and perception, but instead found that the former predicted functional connectivity from the medial prefrontal cortex (mPFC) to the precuneus and inferior parietal cortex, while the latter was predicted by functional connectivity seeded from the aPFC to the cingulate, putamen, and thalamus. However, Baird et al. also examined the differential connectivity strength of aPFC vs mPFC and found that better meta-memory was associated with stronger connectivity between the aPFC and the hippocampus, precuneus,

453 and other memory-related areas, a finding which may possibly explain our mediation results.
454 Thus while these studies suggest a degree of independence between meta-memory and meta-
455 perceptual systems, they also suggest that interactions between memory (precuneus,
456 hippocampus) and metacognition-related (aPFC) brain areas underlie general metacognitive
457 ability.

458 Complementing these results, we found that perceptual metacognitive ability was
459 positively related to the myelo-architectural integrity of the aPFC, as evidenced by coincident
460 AROC-related differences in R_1 and MT maps in this region. In contrast, in the precuneus and
461 left hippocampus we found that decreased MT and increased R_2* were predictive of inter-
462 individual differences in perceptual metacognition. Furthermore, the relationship of
463 microstructure in each of these areas to memory was mediated by metacognitive ability,
464 supporting the hypothesis of an interaction between memory and perceptual awareness. Our
465 results are thus consistent with a general linkage between memory, metacognition, and related
466 neural networks.

467 Although each of the multi-parameter maps have enhanced specificity over
468 conventional weighted imaging and each exhibit sensitivity to particular microstructural tissue
469 properties, this relationship is not unique. Histologically, differences in MT measures strongly
470 correlate with myelin content (e.g., Mottershead et al., 2003; Schmierer et al., 2007; Turati et
471 al., 2015). While myelin is also a significant determinant of R_1 (Koenig, 1991; Mottershead et
472 al., 2003; Gouw et al., 2008), other features of the myelo-architecture such as the axonal
473 diameter, perhaps coupled to the exposed myelin surface, may be a greater determinant, at least
474 in white matter (Harkins et al., 2016). Nonetheless, other factors such as iron content (Gelman
475 et al., 2001; Rooney et al., 2007; Callaghan et al., 2015a) and cellular architecture (Mottershead
476 et al., 2003; Gouw et al., 2008) also play a role. R_2* is highly correlated with iron content
477 (Langkammer et al., 2010) but can also be influenced by fibre orientation and architecture

(Wharton and Bowtell, 2012). Considering this array of factors, we benefit from having a multi-modal view to aid in interpreting our findings. Thus, where we identified a decreased MT coupled with an increased R_2* in the absence of an R_1 effect suggests a coincident decrease in myelin and increase in iron content, potentially driven by changes in underlying microglial and astroglial support structures. In contrast, the co-localisation of increases in both MT and R_1 suggests an increase in myelination independent of changes in iron or other paramagnetic content that would also be expected to impact R_2*.

This pattern of results may suggest a unique neurobiological mechanism for the interaction of stress, memory, and metacognition. One recent study by Reyes et al (2015) tested individual response to stress induction, and then at a later date participant's perceptual metacognitive ability. These authors found that high-stress responders showed an altered overall level of confidence and reduced metacognitive ability. This is particularly interesting in light of our findings in the left hippocampus. The hippocampus is highly sensitive to degradation by prolonged neurotoxic oxidative stress and related inflammation of glial cells (a potential driver of MT), which are responsible for the processing and regulation of cortical iron. Increased iron and decreased MT may thus indicate an adaptive stress response, leading to myelin breakdown (Bartzokis, 2011), such that environmental stress has resulted in elevated neuromelanin levels (Nakane et al., 2008; Chen et al., 2014) to reduce oxidative damage to the hippocampus.

Alternatively, this pattern may be explained by nutritional differences. Glial inflammation is closely linked to iron homeostasis by a complex feedback mechanism, with nutritional iron deficits during foetal, infant, or adolescent development linked to impaired memory and learning (Georgieff, 2008; Carlson et al., 2009, 2010), glial inflammation (Bilbo et al., 2011), and increased risk of neurodegenerative diseases later in life (Gerlach et al., 1994). Iron deficiency exerts numerous effects in the hippocampus and, elevating various metabolites,

GABA, and altering overall tissue architecture and myelination (Jorgenson et al., 2005; Georgieff, 2008). Our results might thus indicate an overall neuro-protective effect, in which reduced hippocampal MT (and increased iron) reflect reduced inflammation of neurobiological support structures, caused by either lower trait-stress response or as the result of increased nutritional iron.

Of course, the causal direction and precise mechanisms underlying these effects remain unclear; it could be for example that individuals with a less stressful environment have a better overall memory (and therefore more evidence of neuroprotective element) (Rodrigue et al., 2013), or the iron profiles indicated here may represent a direct response to stress and/or reflect a neuro-genetic ability to adaptively respond to stress or nutritional challenges. We might speculate that metacognition-related hippocampal histology could potentially be an early biomarker for Alzheimer's and other neurodegenerative diseases; if such a pattern does reflect an early-life response to stress, it may come at the cost of an increased risk to developing these diseases later in life. Regardless, our study provides an interesting starting point for future work, so that we can better understand how the histological factors discovered here relate to metacognitive ability.

Limitations and Future Directions

Methodological limitations common to all studies requiring spatial normalisation are the potential for residual registration errors, as well as partial volume effects. To minimise these sources of bias we used the DARTEL algorithm for inter-subject registration, which results in maximally accurate registration (Klein et al., 2009), and used the voxel based quantification normalisation procedure to minimise partial volume effects introduced by smoothing (Draganski et al., 2011).

Here we speculatively interpret our results as suggesting a link between the histology of the hippocampus and APFC, and the relationship of memory and metacognition. Indeed, the

hippocampus and precuneus are a core part of a memory-related network (Squire, 1992; Brown and Aggleton, 2001). We also found that metacognitive ability both negatively mediated (supressed) the relationship of auditory memory ability and hippocampal/precuneual microstructure, and positively mediated the link between memory and APFC myelination. This suggests that a dynamic interaction between memory and meta-cognition related brain areas mediates the influence of metacognition on memory (or vice versa); however future work with a more general battery of memory and meta-memory tasks is needed to better understand this relationship. Additionally, without stress or nutrition-related measures we can only speculate as to their link with the effects observed here. Indeed, individual differences in brain structure and function are influenced by a variety of developmental, neurogenetic, and environmental factors (Kanai and Rees, 2011).

Thus, an important step for future studies will be to study the microstructural correlates of metacognitive ability with a more comprehensive battery of perceptual, memory, and stress-related measures. Nevertheless, our study is the first to establish that quantitative neuroimaging reveals potential biomarkers sensitive to metacognitive ability, which has allowed us to greatly extend previous functional and volumetric studies. We therefore anticipate that future research will expand upon these findings to better understand their developmental, genetic, and environmental causes.

Conclusion

By using a quantitative multi-parameter mapping approach, we were able to reveal the contribution of the hippocampus and precuneus to perceptual metacognition. Furthermore, as our method yields standardised quantitative metrics sensitive to the underlying tissue microstructure, these results can be used to inform future clinical research as they can be compared directly across research sites. Our results suggest that the concentration of iron in

553 the hippocampus is an important predictor for metacognitive ability, pointing towards a
554 potential neuroprotective mechanism defending introspection from stress. More generally,
555 these results suggest that memory-related systems may be more important than previously
556 realized for the computation of perceptual confidence. Future research into the genetic,
557 environmental, and other dynamic factors underlying these findings are likely to yield strong
558 dividends in the study of metacognitive ability.
559
560 *Acknowledgements:* This work was supported by a Wellcome Trust grant 100227 (MA, GR)
561 and an ERC Starting Grant to DSS (310829). The Wellcome Trust Centre for Neuroimaging
562 is supported by core funding from the Wellcome Trust 091593/Z/10/Z.
563

564 **Tables**

565 **Table 1 – Behavioural Summary**

Table 1
Behavioural Summary

Variable	μ*S* (SD)	σ*S* (SD)	μ (μ*S*,σ*S*) (SD)
d'	1.40 (0.32)	1.60 (0.41)	-0.20 (0.43)
RT (ms)	404.3 (66)	414.0 (69)	409.1 (66)
Accuracy %	73.4 (3.6)	76.8 (4.9)	75.3% (3)
Confidence (1-4)	2.75 (0.26)	2.39 (0.27)	2.56 (0.14)
Confidence (1-100)	73.4 (13.8)	62.6 (15.2)	62.64 (15.23)
AROC	0.68 (0.07)	0.69 (0.08)	0.68 (0.06)
Median μ or σ	6.46 (2.96)	53.34 (13.27)	*na*

566 *Note:* μ*S* = mean staircase, σ*S* = variance staircase, SD = standard deviation.
567

568

569 **Table 2, Summary of Brain Results**

570

Table 2
Summary of Brain Results
VOI Results

Map	Region	k	p_{FWE} peak	p_U peak	*T*	*Z*	x	y	z
MT +	R APFC	38	0.035	< 0.001	4.38	3.92	37	41	22
MT -	R Precuneus	25	0.024	< 0.001	4.54	4.03	10	-58	8
R_2* +	R Precuneus	51	0.040	< 0.001	4.20	3.78	9	-64	24
R_1 +	R APFC	51	0.043	< 0.001	4.25	3.82	37	42	22

Whole Brain Results

Map	Region	k	p_{FWE} cluster	p_U cluster	*T*	*Z*	x	y	z
MT -	L Hippo.	850	0.030	< 0.001	5.48	4.68	-31	-25	-14
R_2* -	L & R V1	598	0.016	< 0.001	4.89	4.28	1	-69	11
R_2* +	L MTG	568	0.011	< 0.001	5.72	4.83	-51	-48	2
R_2* +	R Subiculum†	417	0.044	< 0.001	6.17	5.10	14	-38	-5
R_2* +	L Hippo.‡	5518	< 0.001	< 0.001	4.94	4.31	-26	-36	-13

571 *Note:* Hippo = hippocampus, MTG = middle temporal gyrus, APFC = rostrolateral prefrontal cortex. † indicates
572 peak-corrected result and pvalues. ‡ indicates result from exploratory $p < 0.01$ inclusion threshold. *k* = cluster
573 extent in voxels, T = t-value, Z = z-value, x,y,z = MNI peak coordinates. pFWE cluster = family-wise corrected
574 cluster p-value, pU cluster = uncorrected cluster p-value, pFWE peak = family-wise corrected peak p-value, pU
575 cluster = uncorrected peak p-value. + - indicates positive or negative t-constrast. See *VBQ analysis* and *VBQ*
576 *Results* for more details.

References

Ashburner J (2007) A fast diffeomorphic image registration algorithm. NeuroImage 38:95–113.

Ashburner J (2009) Computational anatomy with the SPM software. Magn Reson Imaging 27:1163–1174.

Ashburner J, Friston KJ (2005) Unified segmentation. NeuroImage 26:839–851.

Baird B, Smallwood J, Gorgolewski KJ, Margulies DS (2013) Medial and Lateral Networks in Anterior Prefrontal Cortex Support Metacognitive Ability for Memory and Perception. J Neurosci 33:16657–16665.

Bartzokis G (2011) Alzheimer's disease as homeostatic responses to age-related myelin breakdown. Neurobiol Aging 32:1341–1371.

Bilbo SD, Smith SH, Schwarz JM (2011) A Lifespan Approach to Neuroinflammatory and Cognitive Disorders: A Critical Role for Glia. J Neuroimmune Pharmacol 7:24–41.

Brown MW, Aggleton JP (2001) Recognition memory: What are the roles of the perirhinal cortex and hippocampus? Nat Rev Neurosci 2:51–61.

Callaghan MF, Freund P, Draganski B, Anderson E, Cappelletti M, Chowdhury R, Diedrichsen J, FitzGerald THB, Smittenaar P, Helms G, Lutti A, Weiskopf N (2014) Widespread age-related differences in the human brain microstructure revealed by quantitative magnetic resonance imaging. Neurobiol Aging 35:1862–1872.

Callaghan MF, Helms G, Lutti A, Mohammadi S, Weiskopf N (2015a) A general linear relaxometry model of R1 using imaging data. Magn Reson Med 73:1309–1314.

Callaghan MF, Josephs O, Herbst M, Zaitsev M, Todd N, Weiskopf N (2015b) An evaluation of prospective motion correction (PMC) for high resolution quantitative MRI. Brain Imaging Methods 9:97.

Callaghan MF, Malik S, Weiskopf N (2015c) Rapid calculation of correction parameters to compensate for imperfect RF spoiling in quantitative R1 mapping.

Carlson ES, Fretham SJB, Unger E, O'Connor M, Petryk A, Schallert T, Rao R, Tkac I, Georgieff MK (2010) Hippocampus specific iron deficiency alters competition and cooperation between developing memory systems. J Neurodev Disord 2:133–143.

Carlson ES, Tkac I, Magid R, O'Connor MB, Andrews NC, Schallert T, Gunshin H, Georgieff MK, Petryk A (2009) Iron Is Essential for Neuron Development and Memory Function in Mouse Hippocampus. J Nutr 139:672–679.

Chen X, Huddleston DE, Langley J, Ahn S, Barnum CJ, Factor SA, Levey AI, Hu X (2014) Simultaneous imaging of locus coeruleus and substantia nigra with a quantitative neuromelanin MRI approach. Magn Reson Imaging 32:1301–1306.

612 Deoni SCL, Peters TM, Rutt BK (2005) High-resolution T1 and T2 mapping of the brain in a
613 clinically acceptable time with DESPOT1 and DESPOT2. Magn Reson Med 53:237–
614 241.

615 Draganski B, Ashburner J, Hutton C, Kherif F, Frackowiak RSJ, Helms G, Weiskopf N
616 (2011) Regional specificity of MRI contrast parameter changes in normal ageing
617 revealed by voxel-based quantification (VBQ). NeuroImage 55:1423–1434.

618 Eickhoff SB, Stephan KE, Mohlberg H, Grefkes C, Fink GR, Amunts K, Zilles K (2005) A
619 new SPM toolbox for combining probabilistic cytoarchitectonic maps and functional
620 imaging data. NeuroImage 25:1325–1335.

621 Fernandez-Duque D, Baird JA, Posner MI (2000) Executive Attention and Metacognitive
622 Regulation. Conscious Cogn 9:288–307.

623 Flavell JH (1979) Metacognition and cognitive monitoring: A new area of cognitive–
624 developmental inquiry. Am Psychol 34:906–911.

625 Fleming SM, Dolan RJ (2012) The neural basis of metacognitive ability. Philos Trans R Soc
626 Lond B Biol Sci 367:1338–1349.

627 Fleming SM, Huijgen J, Dolan RJ (2012) Prefrontal Contributions to Metacognition in
628 Perceptual Decision Making. J Neurosci 32:6117–6125.

629 Fleming SM, Lau HC (2014) How to measure metacognition. Front Hum Neurosci 8
630 Available at: http://www.ncbi.nlm.nih.gov/pmc/articles/PMC4097944/ [Accessed
631 September 30, 2015].

632 Fleming SM, Ryu J, Golfinos JG, Blackmon KE (2014) Domain-specific impairment in
633 metacognitive accuracy following anterior prefrontal lesions. Brain 137:2811–2822.

634 Fleming SM, Weil RS, Nagy Z, Dolan RJ, Rees G (2010) Relating Introspective Accuracy to
635 Individual Differences in Brain Structure. Science 329:1541–1543.

636 Galazka-Friedman J, Friedman A, Bauminger ER (2009) Iron in the brain. Hyperfine Interact
637 189:31–37.

638 Gelman N, Ewing JR, Gorell JM, Spickler EM, Solomon EG (2001) Interregional variation
639 of longitudinal relaxation rates in human brain at 3.0 T: Relation to estimated iron and
640 water contents. Magn Reson Med 45:71–79.

641 Georgieff MK (2008) The role of iron in neurodevelopment: fetal iron deficiency and the
642 developing hippocampus. Biochem Soc Trans 36:1267–1271.

643 Gerlach M, Ben-Shachar D, Riederer P, Youdim MBH (1994) Altered Brain Metabolism of
644 Iron as a Cause of Neurodegenerative Diseases? J Neurochem 63:793–807.

645 Gouw AA, Seewann A, Vrenken H, van der Flier WM, Rozemuller JM, Barkhof F, Scheltens
646 P, Geurts JJG (2008) Heterogeneity of white matter hyperintensities in Alzheimer's
647 disease: post-mortem quantitative MRI and neuropathology. Brain 131:3286–3298.

Harkins KD, Xu J, Dula AN, Li K, Valentine WM, Gochberg DF, Gore JC, Does MD (2016) The microstructural correlates of T1 in white matter. Magn Reson Med 75:1341–1345.

Helms G, Dathe H, Dechent P (2008a) Quantitative FLASH MRI at 3T using a rational approximation of the Ernst equation. Magn Reson Med 59:667–672.

Helms G, Dathe H, Kallenberg K, Dechent P (2008b) High-resolution maps of magnetization transfer with inherent correction for RF inhomogeneity and T1 relaxation obtained from 3D FLASH MRI. Magn Reson Med 60:1396–1407.

Helms G, Draganski B, Frackowiak R, Ashburner J, Weiskopf N (2009) Improved segmentation of deep brain grey matter structures using magnetization transfer (MT) parameter maps. NeuroImage 47:194–198.

Hupé J-M (2015) Statistical inferences under the Null hypothesis: common mistakes and pitfalls in neuroimaging studies. Front Neurosci 9 Available at: http://www.ncbi.nlm.nih.gov/pmc/articles/PMC4333770/ [Accessed February 8, 2016].

Jorgenson LA, Sun M, O'Connor M, Georgieff MK (2005) Fetal iron deficiency disrupts the maturation of synaptic function and efficacy in area CA1 of the developing rat hippocampus. Hippocampus 15:1094–1102.

Kanai R, Rees G (2011) The structural basis of inter-individual differences in human behaviour and cognition. Nat Rev Neurosci 12:231–242.

Klein A, Andersson J, Ardekani BA, Ashburner J, Avants B, Chiang M-C, Christensen GE, Collins DL, Gee J, Hellier P, Song JH, Jenkinson M, Lepage C, Rueckert D, Thompson P, Vercauteren T, Woods RP, Mann JJ, Parsey RV (2009) Evaluation of 14 nonlinear deformation algorithms applied to human brain MRI registration. NeuroImage 46:786–802.

Koenig SH (1991) Cholesterol of myelin is the determinant of gray-white contrast in MRI of brain. Magn Reson Med 20:285–291.

Langkammer C, Krebs N, Goessler W, Scheurer E, Ebner F, Yen K, Fazekas F, Ropele S (2010) Quantitative MR Imaging of Brain Iron: A Postmortem Validation Study. Radiology 257:455–462.

Lorio S, Kherif F, Ruef A, Melie-Garcia L, Frackowiak R, Ashburner J, Helms G, Lutti A, Draganski B (2016) Neurobiological origin of spurious brain morphological changes: A quantitative MRI study: Computational Anatomy Studies of the Brain. Hum Brain Mapp:n/a – n/a.

Lorio S, Lutti A, Kherif F, Ruef A, Dukart J, Chowdhury R, Frackowiak RS, Ashburner J, Helms G, Weiskopf N, Draganski B (2014) Disentangling in vivo the effects of iron content and atrophy on the ageing human brain. NeuroImage 103:280–289.

Lutti A, Hutton C, Finsterbusch J, Helms G, Weiskopf N (2010) Optimization and validation of methods for mapping of the radiofrequency transmit field at 3T. Magn Reson Med 64:229–238.

688 Lutti A, Stadler J, Josephs O, Windischberger C, Speck O, Bernarding J, Hutton C, Weiskopf
689 N (2012) Robust and Fast Whole Brain Mapping of the RF Transmit Field B1 at 7T.
690 PLOS ONE 7:e32379.

691 Maldjian JA, Laurienti PJ, Kraft RA, Burdette JH (2003) An automated method for
692 neuroanatomic and cytoarchitectonic atlas-based interrogation of fMRI data sets.
693 NeuroImage 19:1233–1239.

694 McCurdy LY, Maniscalco B, Metcalfe J, Liu KY, Lange FP de, Lau H (2013) Anatomical
695 Coupling between Distinct Metacognitive Systems for Memory and Visual
696 Perception. J Neurosci 33:1897–1906.

697 Mohammadi S, Carey D, Dick F, Diedrichsen J, Sereno MI, Reisert M, Callaghan MF,
698 Weiskopf N (2015) Whole-Brain In-vivo Measurements of the Axonal G-Ratio in a
699 Group of 37 Healthy Volunteers. Front Neurosci 9 Available at:
700 http://journal.frontiersin.org/Article/10.3389/fnins.2015.00441/abstract [Accessed
701 March 9, 2016].

702 Mottershead JP, Schmierer K, Clemence M, Thornton JS, Scaravilli F, Barker GJ, Tofts PS,
703 Newcombe J, Cuzner ML, Ordidge RJ, McDonald WI, Miller DH (2003) High field
704 MRI correlates of myelin content and axonal density in multiple sclerosis. J Neurol
705 250:1293–1301.

706 Müllensiefen D, Gingras B, Musil J, Stewart L (2014) The Musicality of Non-Musicians: An
707 Index for Assessing Musical Sophistication in the General Population. PLOS ONE
708 9:e89642.

709 Nakane T, Nihashi T, Kawai H, Naganawa S (2008) Visualization of Neuromelanin in the
710 Substantia Nigra and Locus Ceruleus at 1.5T Using a 3D-gradient Echo Sequence
711 with Magnetization Transfer Contrast. Magn Reson Med Sci 7:205–210.

712 Preibisch C, Deichmann R (2009a) Influence of RF spoiling on the stability and accuracy of
713 T_1 mapping based on spoiled FLASH with varying flip angles. Magn Reson Med
714 61:125–135.

715 Preibisch C, Deichmann R (2009b) T1 mapping using spoiled FLASH-EPI hybrid sequences
716 and varying flip angles. Magn Reson Med 62:240–246.

717 Reyes G, Silva JR, Jaramillo K, Rehbein L, Sackur J (2015) Self-Knowledge Dim-Out: Stress
718 Impairs Metacognitive Accuracy. PLoS ONE 10:e0132320.

719 Ridgway GR, Henley SMD, Rohrer JD, Scahill RI, Warren JD, Fox NC (2008) Ten simple
720 rules for reporting voxel-based morphometry studies. NeuroImage 40:1429–1435.

721 Rodrigue KM, Daugherty AM, Haacke EM, Raz N (2013) The Role of Hippocampal Iron
722 Concentration and Hippocampal Volume in Age-Related Differences in Memory.
723 Cereb Cortex 23:1533–1541.

724 Rooney WD, Johnson G, Li X, Cohen ER, Kim S-G, Ugurbil K, Springer CS (2007)
725 Magnetic field and tissue dependencies of human brain longitudinal 1H2O relaxation
726 in vivo. Magn Reson Med 57:308–318.

727 Schmierer K, Tozer DJ, Scaravilli F, Altmann DR, Barker GJ, Tofts PS, Miller DH (2007)
728 Quantitative magnetization transfer imaging in postmortem multiple sclerosis brain. J
729 Magn Reson Imaging 26:41–51.

730 Sinanaj I, Cojan Y, Vuilleumier P (2015) Inter-individual variability in metacognitive ability
731 for visuomotor performance and underlying brain structures. Conscious Cogn 36:327–
732 337.

733 Spence ML, Dux PE, Arnold DH (2015) Computations Underlying Confidence in Visual
734 Perception. J Exp Psychol Hum Percept Perform:No Pagination Specified.

735 Squire LR (1992) Memory and the hippocampus: A synthesis from findings with rats,
736 monkeys, and humans. Psychol Rev 99:195–231.

737 Turati L, Moscatelli M, Mastropietro A, Dowell NG, Zucca I, Erbetta A, Cordiglieri C,
738 Brenna G, Bianchi B, Mantegazza R, Cercignani M, Baggi F, Minati L (2015) In vivo
739 quantitative magnetization transfer imaging correlates with histology during de- and
740 remyelination in cuprizone-treated mice. NMR Biomed 28:327–337.

741 Wager TD, van Ast VA, Hughes BL, Davidson ML, Lindquist MA, Ochsner KN (2009)
742 Brain mediators of cardiovascular responses to social threat, Part II: Prefrontal-
743 subcortical pathways and relationship with anxiety. NeuroImage 47:836–851.

744 Weiskopf N, Callaghan MF, Josephs O, Lutti A, Mohammadi S (2014) Estimating the
745 apparent transverse relaxation time (R2*) from images with different contrasts
746 (ESTATICS) reduces motion artifacts. Brain Imaging Methods 8:278.

747 Weiskopf N, Mohammadi S, Lutti A, Callaghan MF (2015) Advances in MRI-based
748 computational neuroanatomy: from morphometry to in-vivo histology. Curr Opin
749 Neurol 28:313–322.

750 Weiskopf N, Suckling J, Williams G, Correia MM, Inkster B, Tait R, Ooi C, Bullmore ET,
751 Lutti A (2013) Quantitative multi-parameter mapping of R1, PD*, MT, and R2* at
752 3T: a multi-center validation. Brain Imaging Methods 7:95.

753 Wharton S, Bowtell R (2012) Fiber orientation-dependent white matter contrast in gradient
754 echo MRI. Proc Natl Acad Sci 109:18559–18564.

755 Woo C-W, Roy M, Buhle JT, Wager TD (2015) Distinct Brain Systems Mediate the Effects
756 of Nociceptive Input and Self-Regulation on Pain. PLOS Biol 13:e1002036.

757